Insight into Imiquimod Skin Permeation and Increased Delivery Using Microneedle Pre-treatment

Mohammed Hussain Al-Mayahy [a,b] Akmal H Sabri [a], Catrin S Rutland[c], Amy Holmes[d], John McKenna[e] Maria Marlow [a], David J Scurr [a]*

[a.] Division of Advanced Materials and Healthcare Technologies, School of Pharmacy, The University of Nottingham, NG7 2RD, UK

[b.] Department of Pharmaceutics, College of Pharmacy, Al-Mustansiriyah University, Baghdad, Iraq

[c] School of Veterinary Medicine and Science, The University of Nottingham, NG7 2RD, UK

[d.] School of Pharmacy and Medical Sciences, University of South Australia, Adelaide

[e] Department of Dermatology, University Hospitals of Leicester, Leicester Royal Infirmary, Leicester, UK

Email address

*Corresponding author

Dr David Scurr: David.Scurr@nottingham.ac.uk

17

18

19

1. Introduction

Basal cell carcinoma (BCC) is the most common type of skin cancer among Caucasians constituting about 75-80% of skin cancer cases [1]. It has a high prevalence in Europe, Australia and the United States, with approximately 3-4 million cases per year of BCC occur in the United States [2] alone and the incidence rate is rising by 10% annually worldwide [3]. Common aetiologies for BCC are genetic predisposition and exposure to solar radiation (UV light). In addition, increasing age, fair skin with freckles, blond or red hair, blue eyes and male sex represent other risk factors for the condition [4].

The aims of BCC treatment are complete eradication of the tumour with maximum restoration of normal function and acceptable cosmetic outcome via surgical or non-surgical intervention [5]. Non-surgical approaches include radiotherapy, photodynamic therapy and topical treatment with anticancer drugs such as imiquimod (an immune response modifier with antiviral and antitumor activity) or 5-Fluorouracil (an antimetabolite which inhibits DNA replication in cancer cells). Imiquimod has been demonstrated to be more effective in the treatment of superficial BCC and can be used as the first choice treatment [6].

Surgical excision may not be suitable for some patients because of the invasive nature of the treatment, poor cosmetic outcome, cost and waiting times [4]. Conversely, topical treatment with an anticancer drug such as imiquimod provides a non-invasive, self-administered treatment with excellent cosmetic outcome and lower cost. The four major types of BCC based on morphological classification are superficial (15%), nodular (50%), infiltrative (20%) and mixed (15%) [7]. Several clinical studies have demonstrated the efficacy of imiquimod in the treatment of superficial BCC with cure rates range from 87% to 88% for a 6 week treatment course (once daily/ 5 days per week), while the cure rates in nodular BCC range from 42% to 76% for a treatment course of 12 weeks (once daily/ 5 days per week) [8]. As such, the drug is yet to be approved by the FDA for the treatment of nodular BCC. This difference in the clearance rate is attributed to the fact that the lesions in nodular BCC show

deeper invasion within the dermis with an inability of imiquimod to permeate through the dermal layer. Several studies have attributed the poor permeation profile of imiquimod within the dermis is due to its' low water solubility [9]. In addition, the interaction between the amine groups on the drug molecule with the anionic components of the skin may contribute to the poor permeation profile of imiquimod.

Previous studies conducted by Stein *et al.* [10] and Rehman *et al.* [11] assessed the permeation of imiquimod into the skin from Aldara™ cream using HPLC. Stein *et al.* studied the permeation of imiquimod from Aldara™ cream across mouse skin and found that 11.5% of imiquimod from Aldara™ cream permeated across the skin and only 19% remained on the skin surface [10]. Rehman et al. reported a higher amount of imiquimod permeated from Aldara™ cream than from a bigel formulation, where the imiquimod content in the tape strips (TS) from Aldara™ cream was found to be 59.66% of the mean % recovered amount. From both studies imiquimod displayed a high permeability profile from Aldara™ cream into the skin, this can be attributed to the use of mouse skin, since it is thinner and much more permeable than human or pig skin (up to 10 times) [12]. It is also worth noting that in both studies, the researchers employed HPLC to quantify the amount of imiquimod permeated. However, this analysis does not have any imaging capability and therefore it cannot identify the spatial distribution of imiquimod within skin. In the treatment of BCC, uniform distribution is important to ensure complete tumour eradication and hence prevention of future recurrence.

One of the strategies to assist the delivery of topical therapy to deeper BCC is via the use of microneedle technology. Microneedles are arrays of micron-size projections with length ranging between 250-1000 µm providing a minimally invasive means to transport drug molecules into and across the skin. They are composed of small micron sized needles which pierce the skin to create microchannels through which drug molecules can be efficiently delivered [13]. In general,

68 microneedles can be characterised into five main groups, namely solid, coated, dissolving, hollow and
69 hydrogel-forming microneedles [14].These devices confer a minimally invasive and pain-free drug
70 delivery into or across the skin which can improve patient compliance and adherence to treatment.
71 Unlike hypodermic injections, microneedles don't cause bleeding or require trained personnel for
72 administration and can be applied by patients themselves [15].

73 Microneedles have been used to successfully deliver a range of active pharmaceutical agents (APIs)
74 ranging from low molecular weight drugs to macromolecules into and across the skin [15]. Donnelly
75 *et al.* [16] used a silicon microneedle pre-treatment *in vivo* to enhance skin penetration of 5-ALA into
76 mice skin. They found significantly higher levels of the photosensitiser protoporphyrin IX (PpIX) in the
77 microneedle pre-treated skin compared to intact skin. It is postulated that this microneedle pre-
78 treatment drug delivery approach would be a suitable strategy to improve the delivery of imiquimod
79 into the skin to treat BCC lesions.

80 Time-of-flight secondary ion mass spectrometry (ToF-SIMS) is a highly sensitive surface analysis
81 technique that can be used to characterise the surface chemistry of a sample. ToF-SIMS exhibits high
82 chemical specificity and provide chemical imaging data [17]. Furthermore, the preparation of samples
83 for ToF-SIMS analysis is relatively simple and does not require any extraction process that often used
84 in chromatographic methods or the addition of fluorescent tags or radio-labels [18] except the
85 removal of the excess moisture from the samples prior the analysis [19]. Judd *et al*. first used ToF-
86 SIMS to successfully illustrate the permeation of an active agent (chlorhexidine) from 2% w/v aqueous
87 chlorhexidine solution into porcine skin [18]. Sjövall *et al*. also utilised ToF-SIMS to image the
88 distribution of the active pharmaceutical ingredient (API) 'roflumilast' in mouse skin [20]. In addition,
89 Brunelle and co-workers have conducted considerable work on mapping the permeation profile of
90 fatty acids penetration enhancer into the skin highlighting the utility of ToF-SIMS tracking the
91 permeation of exogenous compound into the skin [21–23].

In this study we used an *in vitro* Franz cell with subsequent HPLC and ToF-SIMS analysis to illustrate the permeation depth and lateral distribution characteristics of imiquimod in porcine skin following the application of Aldara™ cream. The same approach was also used to investigate these aspects following a skin pre-treatment using a solid stainless-steel microneedling pen in an attempt to improve the permeation of imiquimod into the skin rendering it more effective in the treatment of deeper nodular type BCC tumours.

2. Materials

Imiquimod was purchased from Bioscience Life Sciences, UK. Aldara™ 5% cream, MEDA Company, Sweden was purchased from Manor pharmacy, UK. Dermapen® which is a microneedling pen was purchased from ZJchao, China. Sodium acetate and isopentane were purchased from Sigma-Aldrich, UK. Acetonitrile (HPLC grade), glacial acetic acid were obtained from Fisher Scientific, UK. Teepol solution (Multipurpose detergent) was ordered from Scientific Laboratory Supplies, UK. D-Squame standard sampling discs (adhesive discs) were ordered from CUDERM corporation, USA. OCT compound were obtained from VWR International Ltd. Belgium. Deionised water was obtained from an ELGA reservoir, PURELAB® Ultra, ELGA, UK. All reagents were of analytical grade, unless otherwise stated. Porcine skin was used to study the permeation profile of imiquimod due to the limited availability and difficulties associated with the use of *ex vivo* human skin. Nevertheless, various studies have highlighted that porcine skin is a suitable alternative due to the similarities in thickness, histological and permeability properties to human skin [24]. Skin samples were prepared from the porcine pig ears of six months old obtained from a local abattoir prior any steam cleaning process. The skin was washed with distilled water and dried using tissue. Hair was carefully cut by scissors to avoid any damage to the *stratum corneum* and the subcutaneous fatty layer was removed using a scalpel. Full skin thickness was used to avoid altering the skin biomechanical properties which may lead to over-penetration of microneedle into the dermal tissue [25]. After that, the full thickness skin samples

were wrapped in an aluminium foil and stored at -20 °C. Skin samples were used within six weeks of being frozen. A skin integrity test was performed by measuring the transepithelial electric resistance (TEER) using a modified form of EVOM2 Voltohmmeter (World Precision Instruments, USA). Skin samples passed the skin integrity test if they showed TEER reading $\geq$ 3 KΩ [26]. TEER measurements were made prior to performing skin permeation experiments.

3. Methods

3.1. Permeation study of Aldara™ cream through porcine skin

Skin samples were mounted on Franz cells with the *stratum corneum* facing upwards. The receptor chamber was filled with 10 mL of 0.1 N HCl used as receptor fluid to keep sink conditions because of the high solubility of imiquimod (basic compound) in this acidic medium 9.5 mg/mL (tested experimentally). Franz cells were then placed in a stirring water bath (Cleaver Scientific Ltd., UK) at 37 °C for 30 minutes to equilibrate before applying the formulation. The skin was dosed with 20 mg of Aldara™ cream on infinite dose basis over an area of 0.64 cm^2. Infinite dose experiments are defined as experiment where the formulation are applied in a manner that ensures continuous excess of test preparation in the donor compartment. This avoid, the concentration of the drug from being the limiting factor for the permeation of the formulation. Infinite dose is achieved when 100 µl is applied per cm^2 for liquid formulations or 10 mg per cm2 for solid or semisolid formulation. Such a volume ensures continuous excess of test preparation in the donor compartment [27]. Such dose will produce fundamental permeation behavior and is frequently utilised when testing the drug permeation profile in the presence of permeability enhancers, in this case the permeability enhancement is attributed to the use of microneedles [28]. .. In order to investigate the utility of microneedles to enhance the permeation profile of imiquimod from commercially available Aldara™ cream, additional Franz cell experiments were performed. However, in this experiment prior to assembling the Franz cells, the

skin was placed on a cork support and the microneedle device was applied vertically on the skin. The microneedle device contains 12 solid (metal) micro sized needles of 32 gauge (230 µm diameter). The length of the microneedles used was 250 µm with a minimum speed of vibration of 1000 turn per minute. The application time was kept to 1 minute with a mild pressure application (thumb pressure). Thereafter, the skin samples were mounted on Franz cells with the *stratum corneum* facing upwards and followed by the application of the same dose of Aldara™ cream. The receptor fluid for the Franz cells were stirred continuously by a small Teflon-coated magnetic stir bar at 600 rpm and the experiment was ran for 24 hours unoccluded. HPLC analysis for imiquimod content from different Franz cells' elements was performed after the 24 hour permeation experiment as detailed in Section 3.4 .

3.2. Insertion study of microneedles and histological examination of microneedle treated skin

To demonstrate the penetration efficiency of the microneedle device, an insertion and staining protocol with *en face* imaging by a light microscope was followed. Porcine skin was pinned onto a flat cork board to stretch the skin and the microneedling pen was applied vertically on the skin. An electronic microneedle device was used to pierce the skin by vibrational motion of microneedles.. These application conditions were used throughout all microneedles experiments. Several drops of gentian violet 1% dye were subsequently applied to cover the treated area and left for 10 minutes. Afterwards, the excess of the dye was removed from the skin surface by a tissue towel and Azo wipes (70% v/v IPA, Synergyhealth, UK). The treated skin area was then examined under light microscope (Leica optical microscope model EC3, Leica Microsystems Ltd., Switzerland) to capture an *en face* image for the microneedles treated skin area.

Following the *en face* imaging of the skin area treated with microneedles by a light microscope, a histological examination was carried out to assess the penetration depth achieved by microneedles. OCT embedding and cryo-sectioning of the skin were performed followed by haematoxylin and eosin staining. Untreated skin samples with microneedles (blank skin) were also subjected to cryo-sectioning, staining and examination under light microscope.

3.3. Tape stripping of porcine skin post-permeation study

After removing the excess cream from the skin surface, the skin was dismantled from the Franz cells assembly and left to air dry at ambient temperature for approximately 2 hours. Following this, a tape stripping technique was employed using adhesive tapes (D-Squame, Standard Sampling Discs, USA) with a diameter of 22 mm. The adhesive tapes were applied and removed successively from the same treated skin area for up to 20 strips with the aid of a roller to press the adhesive tape 10 times onto the skin surface to stretch it to avoid the effects of furrows and wrinkles on the tape stripping procedure. A constant speed was used to remove the adhesive tapes from the skin surface by tweezers (in one swift motion) which were then placed in Eppendorf vials and stored at -20 °C until required for analysis [29].

3.4. Measurement of mass balance and HPLC Analysis

When the Franz cell experiments were completed (after 24 hours), the excess formulation was removed from the surface of the skin by careful application of a combination of very soft dry and moistened sponges with 3% v/v Teepol® detergent solution. The sponges were combined and stored for imiquimod HPLC analysis as a total skin wash. In addition, any cream on the donor chamber inner surface was also removed by the sponges and stored for imiquimod HPLC as a donor chamber wash. The amount of imiquimod from the different Franz cell elements (skin wash, donor chamber wash, pooled tape strips and remaining skin after tape stripping) was extracted by the addition of 20, 10, 5

and 3 mL of methanol extraction mixture (Methanol 90%: Water 9% : 0.1N HCl 1%) respectively. They were then vortexed for 2 minutes and left overnight. Following this, they were sonicated for 30 minutes, filtered through 0.45 µm syringe filter and analysed by HPLC. Receptor fluid samples were filtered through 0.22 µm centrifuge tube filter and injected directly into the HPLC system without any dilution. HPLC analysis was carried out using an Agilent 1100 series instrument (Agilent Technologies, Germany) equipped with degasser, quaternary pump, column thermostat, autosampler and UV detector. System control and data acquisition were performed using Chemostation software. The details of the HPLC chromatographic conditions are as follow: column C_{18} (150 × 4.6 mm) ACE3/ACE-HPLC Hichrom Limited, UK. Mobile phase of buffer: acetonitrile (70:30 v/v), the buffer is of 0.005 M sodium 1-octanesulfonate in water containing 0.1% triethylamine adjusted with dilute perchloric acid to pH of 2.2, flow rate of 0.8 mL/minute, UV detection at λ max. 226 nm, injection volume of 10 µL and column temperature at 25 °C

3.5. Cryotome of porcine skin post-permeation study for ToF-SIMS Analysis

Skin samples removed from Franz cells were placed in a plastic block containing the optimum cutting temperature (OCT) gel (VWR International Ltd., Belgium) which is an inert mounting medium for cryotomy that solidifies upon rapid cooling. Therefore, the plastic block containing skin immersed in OCT was placed in a beaker of isopentane pre-cooled with liquid nitrogen to solidify. After solidification, the OCT blocks were wrapped in aluminum foil, placed in an airtight plastic bags and stored at -80 °C. Cryo-sectioning of skin samples were carried out by placing the OCT block in a cryostat chamber (Thermo Cryotome™, UK) at a temperature of -20 °C. The block was allowed to equilibrate within the cryostat chamber for 30 minutes and then sectioned using a steel blade into vertical cross sections of 20 µm thickness. Following this, the cryo-sections were mounted onto polysine microscope adhesion slides (ThermoFisher Scientific) and freeze dried for 1 hour prior to ToF-SIMS analysis.

3.6. ToF-SIMS analysis

ToF-SIMS was used to analyse individual tape strips and cryo-sectioned skin samples obtained from Franz cell testing. The tape strips and cryo-sectioned skin samples were placed in a freeze dryer for 1 hour prior to ToF-SIMS analysis. ToF-SIMS analysis was performed using a ToF-SIMS IV instrument (IONTOF, GmbH) with a Bi_3^+ cluster source. A primary ion energy of 25 KeV was used, the primary ion dose was preserved below 1×10^{12} per cm^2 to ensure static conditions. Pulsed target current of approximately 0.3 pA, and post-acceleration energy of 10 keV were employed throughout sample analysis. The mass resolution for the instrument was 7000 at m/z 28. The area scanned of the tape strips samples was (9 mm × 9 mm) encompassing the entire skin area exposed to Aldara™ cream during Franz cell diffusion experiments. For the cryo-sectioned skin samples the scanned area was (6 mm × 6 mm) or (10 mm × 4 mm) depending on the section size. All the samples were analysed at a resolution of 100 pixels/mm. An ion representing biological material and therefore indicative of skin (skin marker) was identified as CH_4N^+ and was used to threshold the data sets.. CH4N+ is a common fragment observed in organic materials such as biological specimen. Therefore, this secondary ion was used to track the presence of corneocyte extracted on the tape strips. After that, the data was reconstructed to remove the data from the adhesive tape material found between the fissures in the stripped skin (removing the substrate data) and therefore the data was only analysed from the skin material. Following this, each image of the individual tape strip (9 mm × 9 mm) was divided into four smaller data sets of (4.5 mm × 4.5 mm) which results in four repeats (n = 4) for each sample and their intensities were normalised to the total ion intensity. In addition, pure imiquimod and Aldara™ cream reference spectra were obtained by analysing the pure drug and the cream on silicon wafer using ToF-SIMS.

4. Results and Discussion

4.1. Measurement of mass balance and HPLC Analysis of Aldara permeation from porcine skin.

The mean total recovery for mass balance of imiquimod recovered from the different Franz cell components following the permeation study of Aldara™ cream is graphically illustrated in Figure 1. The recovery percentage of applied dose is highest in the skin wash (90 %) as compared to other components indicating that the imiquimod delivered from Aldara™ cream has limited permeation into the skin. A very minor amount (< 1 %) was recovered from the remaining skin, suggesting that imiquimod permeation from Aldara™ cream is very limited and is consistent with the FDA approval details and clinical trials that showed the efficacy of Aldara™ cream just for the treatment of superficial BCC lesions [30,31].

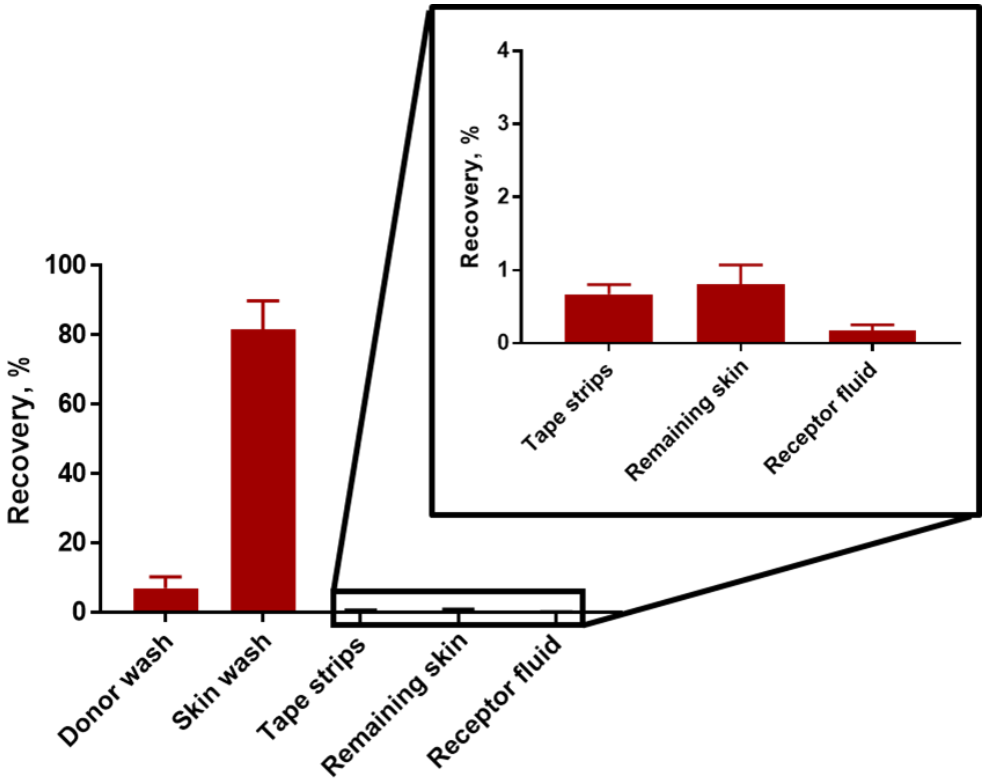

244

245 *Figure 1 Mean total recovery for mass balance of applied dose amount of imiquimod from the different Franz cell components*
246 *(donor chamber wash, skin wash, tape strips, remaining skin and receptor fluid) of the permeation study of Aldara™ cream*
247 *when analysed by HPLC. Data is presented as the mean ± SD (n = 6). The inset provides details on the amount of imiquimod*
248 *that have permeated into (tape strips and remaining skin) and across (receptor fluid) the skin.*

249 The amount of imiquimod observed to permeate in this study is less than that observed by Stein *et al.*
250 who found 11.5 % in the skin for imiquimod from Aldara™ cream and only 19% remained on the skin
251 surface when analysed by HPLC [10]. This higher imiquimod permeability observed by Stein *et al.* can
252 be attributed to the use of mouse skin, since it is thinner and much more permeable than human or
253 pig skin (up to 10 times) [32,33].

254 The high lipophilicity and low aqueous solubility of imiquimod suggests that it may have easier
255 permeation into the *stratum corneum* layer compared with the more aqueous viable epidermis and
256 therefore it may form a depot within the *stratum corneum* since the viable epidermis has a high-water
257 content. Several studies have shown that lipophilic drugs and lipophilic UV filters tend to be preferably
258 located or accumulated on the skin surface and in the superficial layers of the *stratum corneum*

[34,35]. Using porcine skin, as a suitable alternative to human skin, the current results are in agreement with these findings and highlight the superficial permeation of imiquimod into the skin. Such finding further corroborate the licensing restriction imposed by the FDA on Aldara™ cream for the treatment of superficial BCC over the nodular variants. Although the HPLC analysis provide useful quantitative results, the analytical technique does not confer any detail regarding imiquimod distribution within individual layers of skin. Therefore, additional analytical techniques were explored in an attempt to provide such spatial detail regarding imiquimod permeation.

4.2. ToF-SIMS analysis of tape strips post permeation study

Due to the several advantages offered by the ToF-SIMS outlined in Judd *et al* [18]., this technique was implemented in this study to glean a more detailed insight into permeation of imiquimod from Aldara™ cream including an analysis of individual tape strips and imaging of the chemical distribution of imiquimod at their surface. Prior to ToF-SIMS analysis of the tape stripped, some preliminary ToF-SIMS experiments were performed to obtain reference spectra of pure imiquimod and Aldara™ cream. ToF-SIMS survey spectra of pure imiquimod and Aldara™ cream reference on silicon wafer in positive polarity are shown in Figure 2 (a) and (b) respectively.

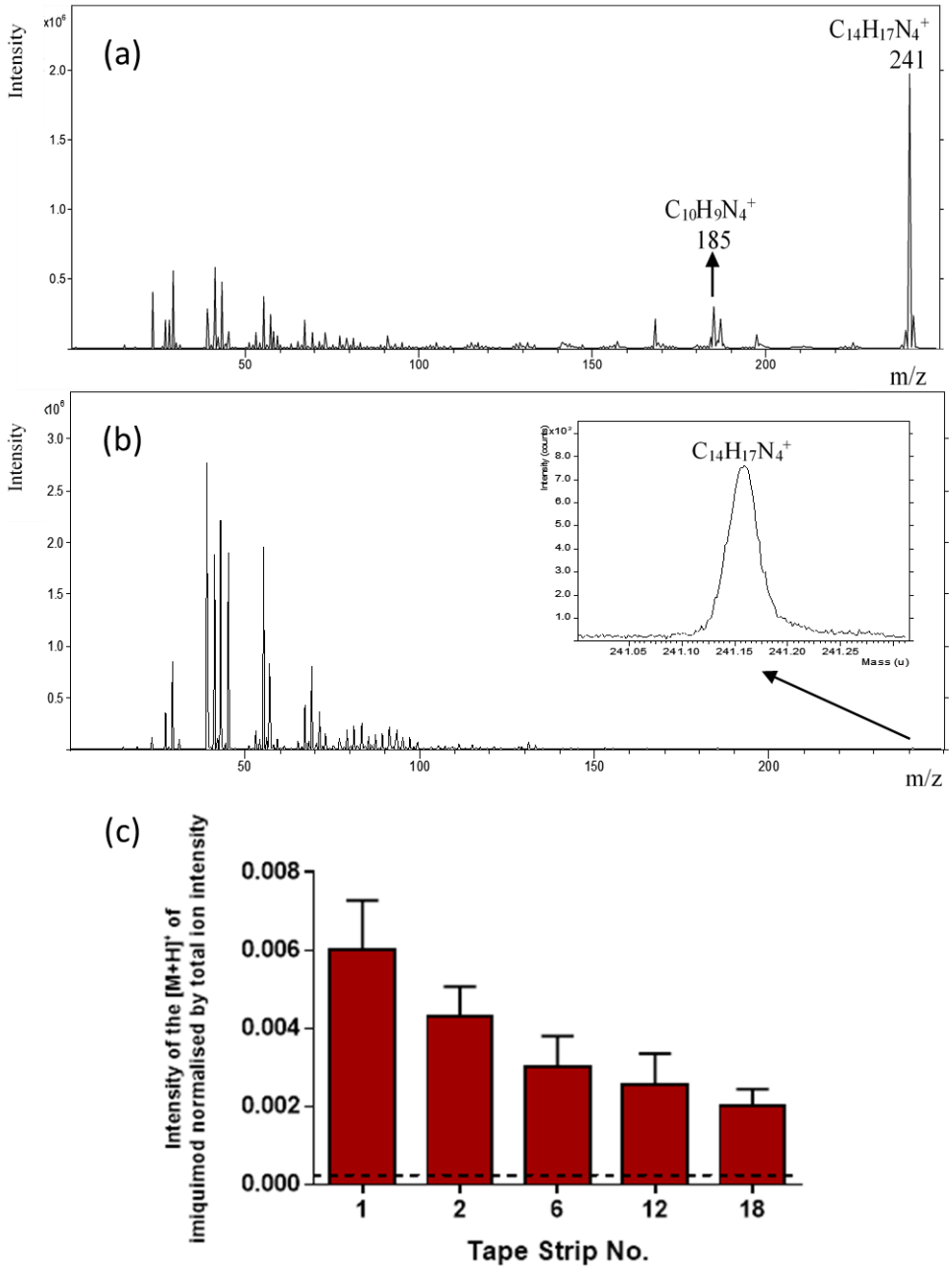

274

275 *Figure 2 Positive polarity ToF-SIMS survey spectra of (A) imiquimod reference and (b) Aldara™ cream, where the inset spectrum*
276 *shows the peak of the $[M+H]^+$ of imiquimod at m/z = 241. (c) Ion intensity values of the $[M+H]^+$ of imiquimod in Aldara™ cream*
277 *tape strips normalised by total ion intensity. Data is presented as the mean ± SD (n = 4). The dotted black line represents the*
278 *ion intensity obtained from the control skin samples.*

279

280

281 As shown in Figure 2 (a), two secondary ion peaks relevant to imiquimod are observed in the positive

282 polarity spectra, the molecular ion $[M+H]^+$ peak of imiquimod $C_{14}H_{17}N_4^+$ (m/z = 241) and the fragment

ion peak $C_{10}H_9N_4^+$ (*m/z* = 185). The $[M+H]^+$ of imiquimod $C_{14}H_{17}N_4^+$ which resulted from the ionisation of the whole imiquimod molecule $C_{14}H_{16}N_4$ (M.wt. 240) is more intense than the fragment ion peak. In the negative polarity only a fragment ion peak, $C_{10}H_8N_4^-$ (*m/z* = 184), is observed (Supporting Information, Figure S1). The positive polarity data is therefore considered to be more informative than the negative polarity due to the presence of the $[M+H]^+$ at a relatively high intensity which provides unambiguous identification of imiquimod. Therefore, the ToF-SIMS data of imiquimod will be presented in the positive mode only.

The ToF-SIMS survey spectrum of Aldara™ cream is shown in Figure 2 (b). Although the peak of the $[M+H]^+$ of imiquimod in Aldara™ cream is not as intense as observed for the pure imiquimod reference material Figure 2 (a), it is clearly resolved suggesting that ToF-SIMS can be used to identify imiquimod in Aldara™ cream.

To assess the exact permeation of imiquimod and visualise its distribution within the *stratum corneum*, tape strips obtained from Franz cell experiments were analysed by ToF-SIMS. The secondary ion intensity data for the $[M+H]^+$ ion of imiquimod in Aldara™ cream treated skin tape strips are shown in Figure 2 (c) whereby it can be observed that this ion is observed above the control intensity throughout the series of 18 tape strips (therefore approximately illustrating the full depth of the *stratum corneum*). A decreasing ion intensity is observed from the outer surface of the skin (TS 1) to the inner layers of the *stratum corneum* (TS 18). The ability of the ToF-SIMS to analyse single tape stripped skin samples (layer by layer of skin analysis) to map the permeation of imiquimod within the *stratum corneum* has not been previously observed and this study provides further insight into the exact depth of permeation achieved with this drug. This decreasing permeation of imiquimod at the inner layers of the *stratum corneum* is consistent with the HPLC results that demonstrated a limited permeation of imiquimod into the deeper skin layers (less than 1% recovered from the remaining skin specimen).

ToF-SIMS ion images of the entire tape stripped area, which represents the whole exposed area of the skin to Aldara™ cream during Franz cell diffusion experiment (9 mm diameter), are illustrated in Figure 3. The total, skin marker (CH_4N^+), and imiquimod marker ($C_{14}H_{17}N_4^+$) ion images are shown in Figure 3 (a, b and c respectively. The intensity are scaled to the same value to enable a valid or fair comparison.

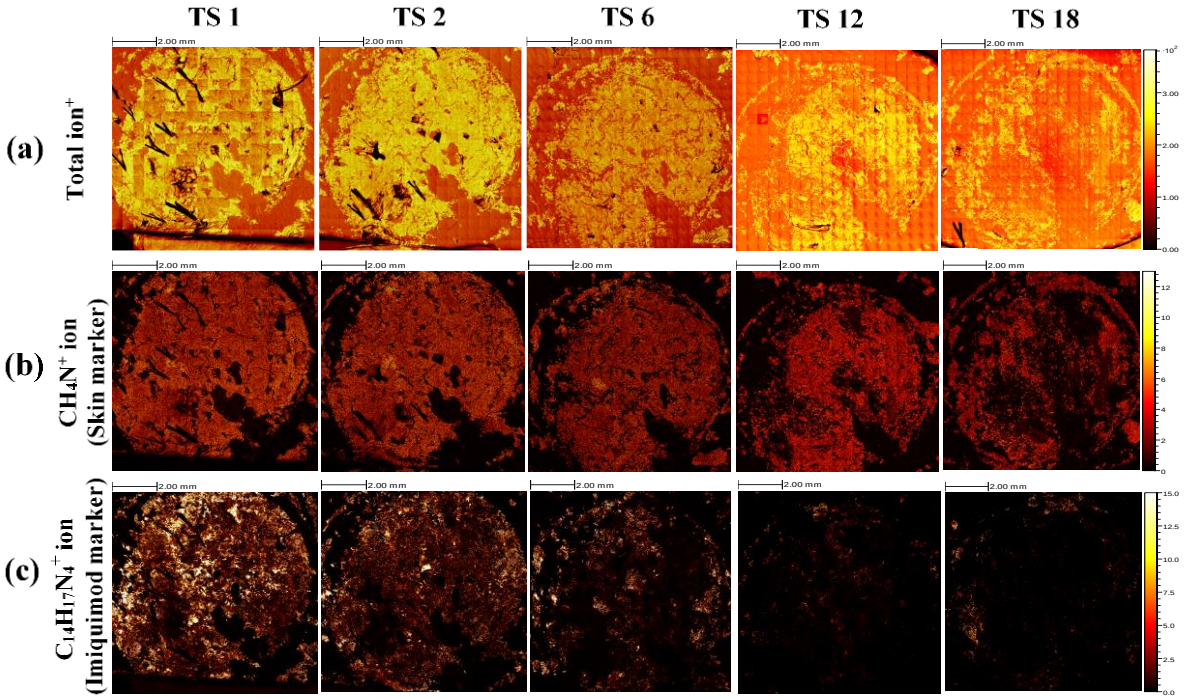

Figure 3 ToF-SIMS ion images of Aldara™ cream treated skin tape strips showing the (a) the total (b) skin marker (CH_4N^+) and (c) imiquimod marker ($C_{14}H_{17}N_4^+$) ions. The scanned area is (9 mm × 9 mm).

An examination of the skin marker, CH_4N^+ (Figure 3 (b), shows that the amount of skin (corneocytes) attached per tape strip is reduced moving from the outer skin surface (TS 1) towards the inner layers of the *stratum corneum* (TS 18). Although there is some reduction, the significant reduction appears to occur at around TS 12 and that TS 1, 2 and 6 show a large amount of stripped corneocytes. This would be anticipated and similar observations of decreasing skin amount from the upper to lower tape strips have been reported by other studies when corneocytes on tape strips were determined by different methods such as the weighing method, protein assay method and UV/visible method. This

is due to the increased cohesion between the cells at the deeper *stratum corneum* layers compared to the outer layers which results in reduced amounts of skin being removed by a tape strip [36–38].

The ion images of the $[M+H]^+$ of imiquimod (Figure 3c) are observed to decrease from the uppermost layer (TS 1) towards the deeper layer of the *stratum corneum* (TS 18) correlating with the ion intensity data shown in Figure 2 (c). Although TS 1 and 2 show a non-uniform distribution of the $M+H^+$ ion, there are very few instances where the $M+H^+$ ion is not present coincident with the skin marker. This suggests that within the first two layers of skin the imiquimod has permeated significantly and would potentially explain its ability to successfully treat superficial BCC tumours. The skin marker for TS 6 shows some reduction in the amount of skin removed but nonetheless still shows most of the Franz cell area. The ion distributions within TS 6 exhibit some areas where the $M+H^+$ for imiquimod and the skin marker do not correlate, where the $M+H^+$ for imiquimod is absent. It is proposed that although imiquimod has permeated to this layer of the skin, it has not done so uniformly with absent patches up to several millimetres in diameter. It is evident from the skin marker ion that TS 12 and 18 exhibits significantly less skin than previous strips, however, it is clear that relatively little of the $M+H^+$ ion of imiquimod can be observed correlating with the location of the skin. It is proposed that some imiquimod has permeated to the lower region of the *stratum corneum*, however, it has done so in very small areas often no larger than 1 mm in diameter.

This observed non-uniform distribution of imiquimod within skin from TS 6 onwards can decrease the efficacy of Aldara™ cream to effectively treat whole BCC lesions. The pattern of drug distribution within the skin layers is very important in BCC because the whole lesion area should be treated evenly at the effective concentration to ensure complete cure and prevent recurrence. Therefore, the ability to assess this is of great importance, since the topical treatment of BCC lesions with Aldara™ cream has shown higher recurrence rate in comparison to surgery [8], particularly tumours with thickness > 0.4 mm [39]. These findings show detailed permeation of imiquimod down to TS 18. The non-uniformity

346 in later layers supports the rationale of why FDA restrict the license of Aldara™ for the treatment of
347 superficial BCC over nodular BCC.

348 4.3. Insertion study of microneedles and histological examination of microneedle
349 treated skin

350 Given the limited permeation profile of imiquimod when applied as a topical cream, the utility of a
351 skin pre-treatment using a microneedle pen as a permeation enhancement strategy was pursued.
352 However, prior to this, the insertion profile of the device was investigated. The image of the 12-metal
353 microneedle cartridge that is fixed in the microneedle device is shown in Figure 4 (a). The diameter of
354 the base (circular shape) containing the 12 microneedles is 5 mm and the distance between each
355 microneedle pin is approximately 1.5 mm.

356 To demonstrate the efficiency of the microneedle device to penetrate the uppermost layer of the skin,
357 *en face* imaging by light microscopy was performed for the porcine skin samples treated with the
358 microneedles and stained with gentian violet as illustrated in Figure 4 (b). These images show that the
359 dyes are appropriately retained in the microchannels formed by the microneedles. This indicates the
360 capability of the microneedles to successfully pierce the skin.

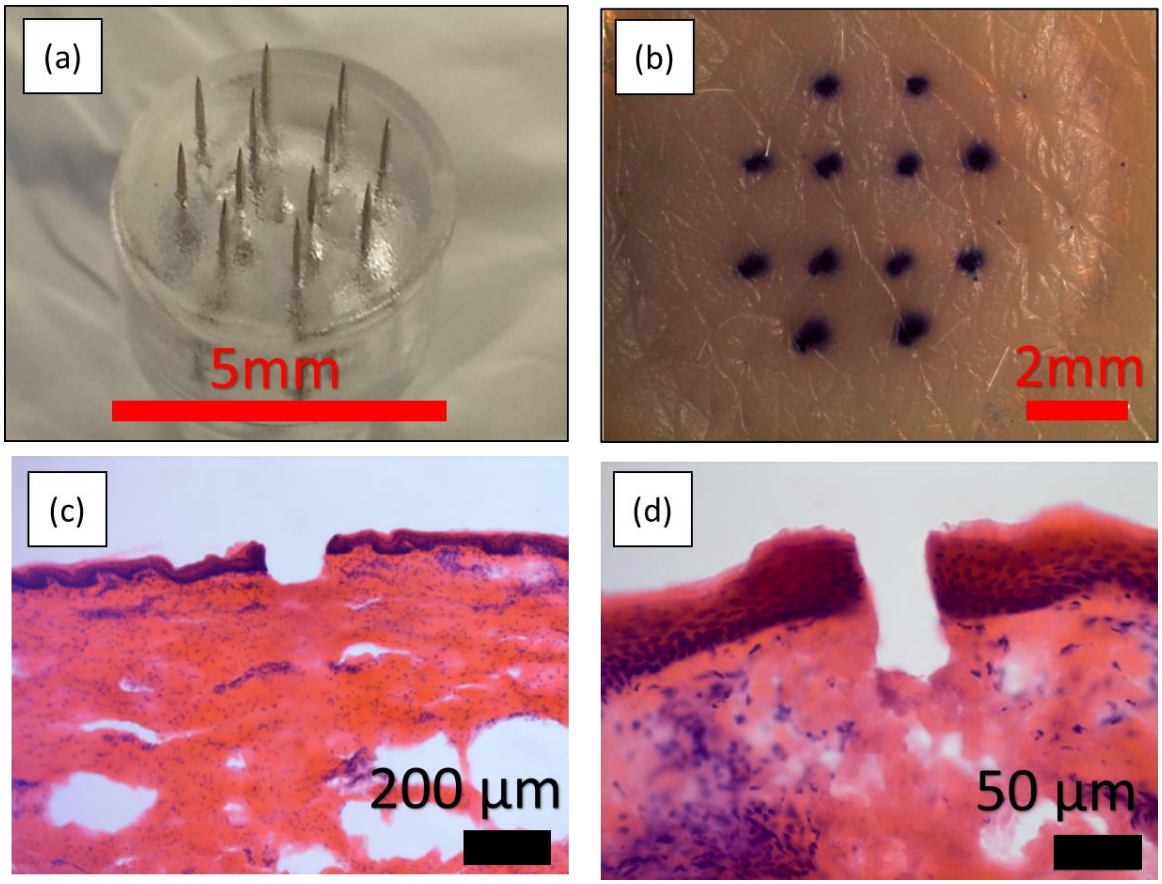

Figure 4 En face images of (a) the microneedles cartridge fixed in the microneedle device used to pierce the skin, (b) porcine skin following microneedle device treatment and staining with gentian violet. (c) Light microscope images H&E stained cross-sections identifying the location of the microchannels within skin tissue (d) H&E stained cross-sections but at a higher magnification.

The microneedling pen penetration efficiency was observed to occur in a reproducible manner throughout the tested skin samples which can be attributed to the fixed velocity used in the microneedles insertion provided by the microneedle device. Verbaan *et al*. demonstrated that the use of an electrical applicator for microneedles with 300 µm length at certain velocity facilitates the insertion of the microneedles into the skin in a reproducible manner compared to manual application [40]. The stained cross-sections with H&E highlight the location of the microchannels within skin tissue and it can be observed that the microneedles penetrate the *stratum corneum* and viable epidermis to reach the papillary dermis (PD) layer (the layer located directly beneath the viable epidermis). In order to measure the pore size, the diameter of the stained pores could be measured to provide an estimate

of the size of the microchannels formed. However, as diffusion may occur, a more accurate way to estimate the pores diameter is to cryo-section the skin samples directly following insertion and measure the channel diameter via microscopy. It can be seen from Figure 4 b that the measured diameter of the pores ranged from 300 to 500 µm. However, these values are in contrast to the measured values from the cryo-sectioned samples (Figure 4 c and d) that showed the diameter of the pores to be between 40 and 95 µm. This overestimation of the pore size is thought to be due to the lateral diffusion of the dyes to the surrounding dermal tissue. An apparent limitation of the *en face* imaging method of visualising microneedles treated skin is the overestimation of the pore diameter because of the lateral diffusion of the dyes [41,42]. In addition, a recent study conducted by Coulman *et al.* highlighted that such overestimation may also arise from tissue processing steps which influence tissue hydration and elasticity of the skin [42]. However, such overestimation will not affect the goal of the study which is to use the microneedling pen to breach the *stratum corneum* in order to generate conduits to promote the delivery of imiquimod into the skin. A noteworthy point is that the microneedle cartridge fixed to microneedle device is disposable and can be used just for one application and then replaced with a new one for the next sample. This diminishes any damage that may occur to the integrity of microneedles from repeated applications and increases the microneedles penetration reproducibility. Simultaneously, from the clinical perspective this eliminates any safety issue generated from the breaking of the microneedles within skin from the reuse of the same microneedles.

.

4.4. Mass balance measurement and HPLC Analysis of Imiquimod from Aldara™ application on microneedle pre-treated skin.

The mean percentage recovered amounts of imiquimod from the different Franz cell elements of the permeation study of Aldara™ cream with and without microneedles pre-treatment are reported in Table 1. It is observed in Table 1 that the mean percentage recovered amount of imiquimod from tape strips and remaining skin elements of Aldara™ cream with microneedles pre-treatment is approximately three times higher than the Aldara™ cream alone. This provides a greater opportunity for the cream to more efficiently treat whole superficial or nodular BCC lesions. In addition, the statistical comparison between the recovered amounts of imiquimod in the remaining skin shows that the recovered amount of imiquimod with microneedle pre-treatment is significantly higher (Unpaired Student's *t*-test $p<0.05$) than the Aldara™ cream alone as illustrated in Figure 5.

Table 1 Mean percentage recovered amount of imiquimod from the different Franz cell elements of the permeation study of Aldara™ cream with and without microneedle pre-treatment when analysed by HPLC. Data is presented as the mean % ± SD (n = 6)

Analysed Element	Aldara™ cream only (mean % recovery ± SD)	Aldara™ cream with microneedles pre-treatment (mean % recovery ± SD)
Donor wash	7.11 ± 3.27	9.38 ± 4.59

Skin wash	81.72 ± 8.14	72.39 ± 12.02
Tape strips	0.67 ± 0.13	2.38 ± 2.40
Remaining skin	**0.81 ± 0.26**	**2.27 ± 0.39**
Receptor fluid	0.17 ± 0.08	1.89 ± 0.47

413

414

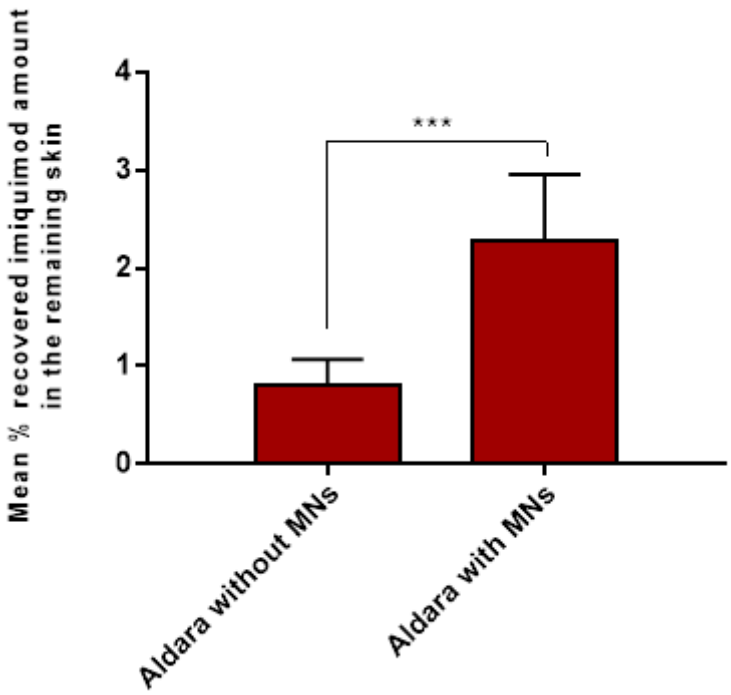

415

416 *Figure 5 Mean percentage recovered imiquimod amount in the remaining skin of the permeation study of Aldara™ cream*
417 *with and without microneedle pre-treatment when analysed by HPLC. Data is presented as the mean ± SD (n = 6). Unpaired*
418 *Student's t-test p<0.05*

419

Furthermore, it is observed that with microneedle pre-treatment the imiquimod's amount in the receptor fluid is approximately ten times higher than the Aldara™ cream alone. This increase in the recovered amount of imiquimod in the receptor fluid is perhaps anticipated since the microchannels created by microneedles can reach the depth of the papillary dermis layer and thus higher amounts of imiquimod bypass the skin barriers and are presented in the receptor fluid. For *in vivo* conditions, this would suggest that higher amounts of imiquimod would be available for systemic circulation which may lead to increase the risk of imiquimod's systemic adverse effects. However, in BCC patients the *stratum corneum* becomes thicker because of the hyperkeratinisation associated with the tumour lesions [30] and the microchannels created by microneedle device may not reach the depth of papillary dermis and hence less amounts of imiquimod would be available for systemic absorption. Besides that, it could be argued that the utilisation of such device may push cancerous cells from superficial BCC into the dermis leading to the potential risk of seeding and spreading the cancer cell in a new dermal microenvironment. However, the propensity for such phenomenon is minimal due to the nature of BCC cells which is highly dependent on its microenvironment for survival[43]. However, in an attempt to limit the likelihood of such side effect, the use microneedle device could be reserved only for deeper BCC lesions such as those seen in nodular and infiltrative BCC.

4.5. ToF-SIMS Analysis of Tape Strips from skin pre-treated with microneedles and subsequent Aldara™ cream application

ToF-SIMS analysis of the tape strips of Aldara™ cream on microneedle pre-treated skin shows a significant increase in the ion intensity of the $[M+H]^+$ of imiquimod in tape strips 2, 5 and 10 h for the microneedles pre-treatment samples as shown in Figure 6 (a). This indicates that a higher amount of imiquimod had permeated into the *stratum corneum* following microneedles application which is in accordance with the HPLC results (Table 1).

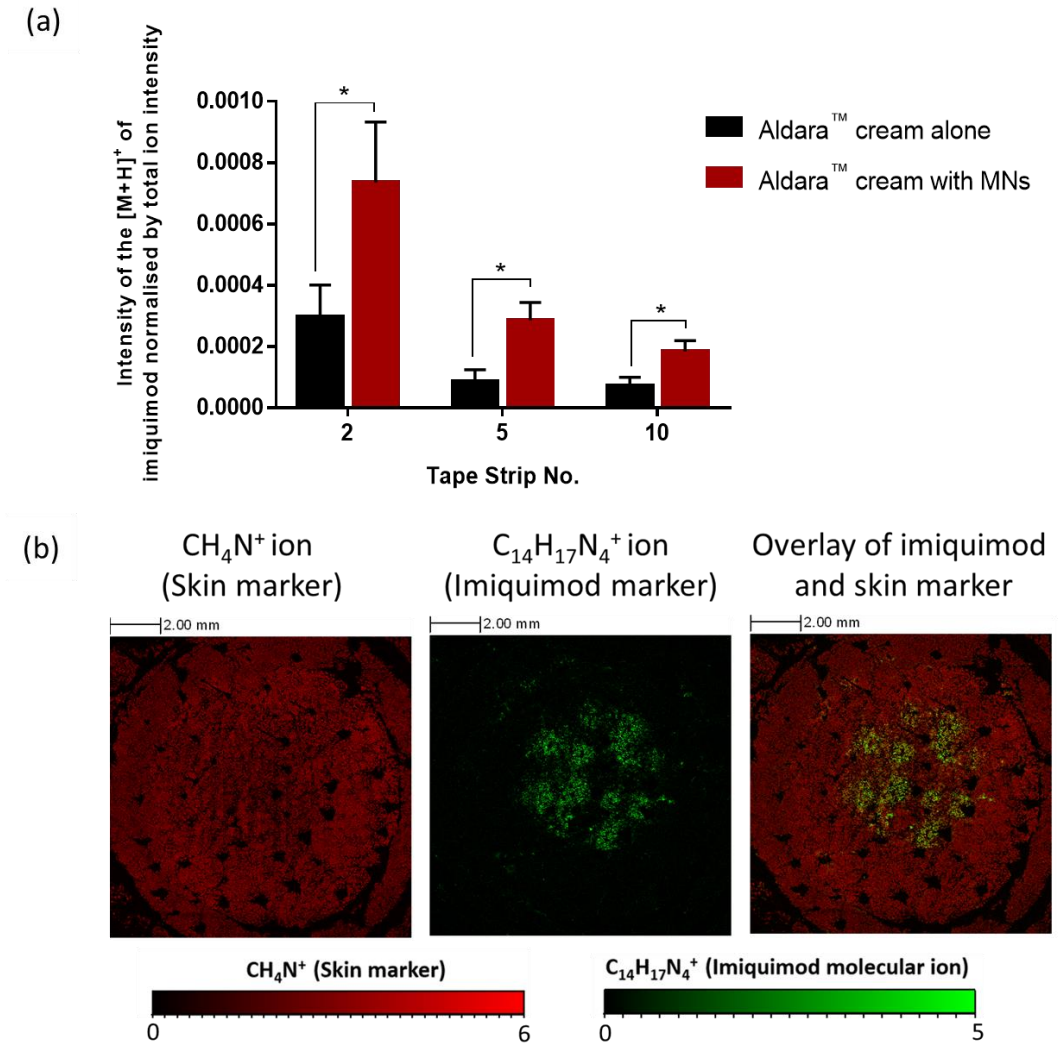

Figure 6 a) Ion intensity values of the [M+H] + of imiquimod ($C_{14}H_{17}N_4^+$) in Aldara™ cream tape strips (2, 5 and 10) with and without microneedles pre-treatment normalised by total ion intensity. Data is presented at the mean ± SD (n = 4). Unpaired Student's t-test p<0.05 (b) ToF-SIMS ion images of tape strip two of Aldara™ cream with microneedles pre-treatment showing: the skin marker (CH_4N^+), the imiquimod marker ($C_{14}H_{17}N_4^+$), and the overlaid image of imiquimod (green colour) and the skin (red colour). The scanned tape strip area is of 12 × 12 mm².

ToF-SIMS ion images of tape strip two of Aldara™ cream with microneedles pre-treatment are shown in Figure 6 (b). It can be seen that the pattern of imiquimod distribution follows the pattern of the microneedle array on the derma pen (Figure 4 (a)). In addition, imiquimod is mostly localised in the area disrupted by the application of the microneedle device (i.e. at a circular region in the middle of the tape strip which corresponds to the shape of the microneedle device cartridge). Figure 6 (b) also shows that imiquimod ion, highlighted in green, laterally diffuses out of the microchannels and distributes to the peripheral epidermal tissue. Such findings indicate that the utilisation of

456 microneedling pen in tandem with Aldara™ cream application is able to promote lateral permeation
457 of drug to surrounding skin tissues. Such apparent lateral permeations have been observed by various
458 groups using conventional techniques such as fluorescent microscopy. These groups have attributed
459 that the observed lateral permeation is due to the overlapping drug diffusion fronts from individual
460 microneedle sites [44,45]. However, it there is yet any research to date that have observed
461 enhancement in lateral permeation using ToF-SIMS.

462

463 ## 4.6. ToF-SIMS Analysis of Skin Cross-sections

464 ToF-SIMS analysis of cryo-sectioned skin samples were used to map imiquimod permeation within
465 different skin layers. Skin cross-sectioning can be used as a complementary tool to the tape stripping
466 technique to follow and visualise drug permeation within skin. ToF-SIMS analysis of the cryo-sectioned
467 skin samples shows that the ion intensity of the $[M+H]^+$ imiquimod from Aldara™ cream with
468 microneedle pre-treatment is significantly higher than the ion intensity obtained from the samples
469 without microneedles pre-treatment as shown from their overlaid spectra (Supporting Information
470 Figure S2). This corresponds with the data obtained by tape stripping shown in Figure 6 (a). It is
471 thought with the presence of the microchannel created by microneedles application, imiquimod
472 penetration is not only restricted to the microchannel site but it radiates to the adjacent tissue (lateral
473 distribution as observed in Figure 6 (b)) which results in almost continuous higher intensity zones of
474 imiquimod localised at the upper skin strata.

475 The whole ToF-SIMS ion images of the cryo-sectioned skin samples of Aldara™ cream with
476 microneedles pre-treatment are illustrated in Figure 7 which show the total and the overlay image of
477 the skin marker, CH_4N^+ with imiquimod molecular ion $C_{14}H_{17}N_4^+$ (Figure 7 a and b respectively) . An
478 examination of the total ion image and the skin marker image indicates the location of the
479 microchannels within the skin sections (white arrows in Figure 7 (a and b)) created by the application

480 of microneedles. The $[M+H]^+$ imiquimod ion image shown in the overlay image (Figure 7 (b)) highlights
481 the distribution of imiquimod at the upper layer of the skin sections in addition to its localisation in
482 the microchannels. It is apparent from that there are some indentations in the skin that may have
483 formed upon microneedle application. However, not the entire top layer of the cross-section contains
484 such indentations despite the entire section of the skin analysed covers the entire microneedle treated
485 region. This may be due to the viscoelastic nature of the skin that causes some region of the skin to
486 recoil and recover over time from the indentations formed from microneedle application.
487 For evaluating the difference between the two treatments in Figure 7 (b), it is worth highlighting that
488 the imiquimod signal arising from the SC is of great interest for the comparison. From the figure it is
489 evident that there is limited availability of imiquimod within the skin layers when applied as a topical
490 cream alone. However, when Aldara™ is applied to the microneedle pre-treated skin, we can observe
491 that imiquimod is mostly located in the *stratum corneum* which makes imiquimod available in this
492 layer. Such observation would suggest lateral permeation of imiquimod following cream application
493 on microneedle treated skin which further supports Figure 6. It is clear here that the imaging capability
494 of ToF-SIMS illustrates where the drug is localised within the skin tissues. Such findings may be of
495 heuristic value in guiding the development of such systems in order to improve intradermal delivery
496 of therapeutics. However, we are unable to see imiquimod in deeper layer using cross-sections as the
497 drug is diluted over a wide area of the dermis and epidermis. In comparison, the HPLC data from Table
498 1 suggest increased intradermal delivery with microneedle skin pre-treatment. Such imiquimod
499 detection was achieved as the extraction procedure concentrates imiquimod from the remaining skin
500 allowing detection with the HPLC instrument.

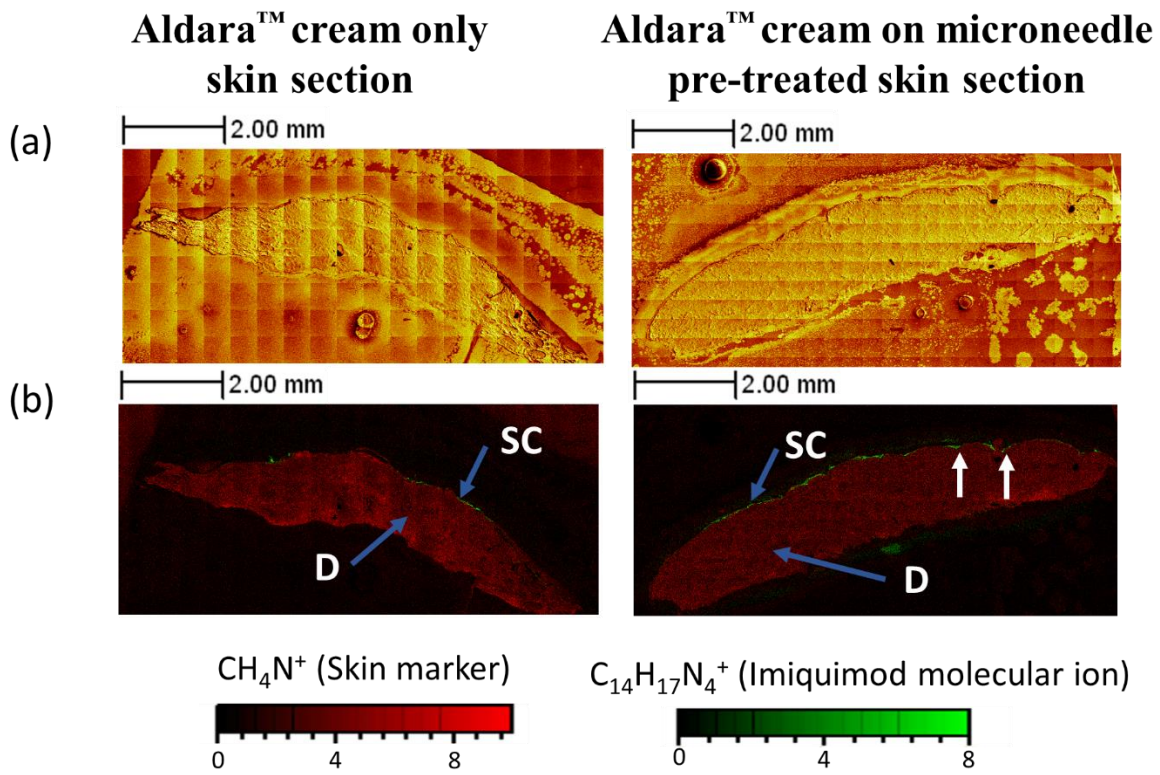

Figure 7 ToF-SIMS ion distribution map of porcine skin cross sections from Aldara™ cream on intact skin and microneedles pre-treated skin. (a) the total ion$^+$, (b) an overlay image of the skin marker (CH_4N^+) with imiquimod marker ($C_{14}H_{17}N_4^+$) to indicate the localisation of imiquimod within the stratum corneum. SC indicates stratum corneum, D indicates dermis. White arrows indicate microneedle indentation into the skin that still persist after 24 hours. The skin cross-section covers the microneedle-treated part of the skin as the microneedle array is 5mm wide.

The HPLC and ToF-SIMS results of Aldara™ cream with microneedles pre-treatment quantitatively and qualitatively demonstrate increased delivery of imiquimod into the epidermal skin layers and suggest its potential usefulness for more efficient treatment of both superficial and nodular BCC lesions. In addition, both the Aldara™ cream and the microneedle device are commercially available systems making them easily accessible. This study is considered to be a proof-of-concept analysis providing an insight into the potential use of microneedles for improving imiquimod's skin penetration and further

ex vivo and *in vivo* investigation on human skin with BCC lesions are required to optimise the final application conditions.

5. Conclusion

The current work demonstrates a novel application of Franz diffusion cells, skin tape stripping and skin cryo-sectioning with subsequent analysis by HPLC and ToF-SIMS to map and visualise the distribution of imiquimod into the skin from the commercial product Aldara™. The ToF-SIMS ion images of Aldara™ cream tape strips illustrated a non-uniform distribution of imiquimod within deeper skin strata which is consistent with the FDA approval and clinical trials for the treatment of superficial BCC. In addition, this study also highlights the potential advantages of solid microneedles skin pre-treatment in conjugation with Aldara™ cream application to enhance delivery of imiquimod into the epidermal layers of the skin for the treatment of the deeper and more invasive nodular BCC lesions. This work also demonstrates the heuristic value and complementary role of ToF-SIMS technique in the analysis and imaging of imiquimod permeation into the skin with high sensitivity and chemical specificity without the need of fluorescent tags or radiolabels.

Acknowledgements

This work was supported by the Ministry of Higher Education in Iraq for sponsoring the PhD study of Mohammed Hussain Al-Mayahy. This work was also supported by the Engineering and Physical Sciences Research Council (EPSRC) [grant number: EP/L01646X/1] via a PhD sponsorship for Akmal Sabri; at the Centre for Doctoral Training for Advanced Therapeutics and Nanomedicine at the University of Nottingham. We would like to thank Dr Mark Prausnitz from Georgia Tech School of Chemical and Biomolecular Engineering for his insightful discussion and advice provided on the use of gentian violet to locate microneedle channels.

Conflict of Interest

Conflicts of interest: none.

References

[1] T.L. Diepgen, V. Mahler, The epidemiology of skin cancer., Br. J. Dermatol. 146 Suppl 61 (2002) 1–6. http://www.ncbi.nlm.nih.gov/pubmed/11966724 (accessed August 18, 2018).

[2] M. Alam, L.H. Goldberg, S. Silapunt, E.S. Gardner, S.S. Strom, A.W. Rademaker, D.J. Margolis, Delayed treatment and continued growth of nonmelanoma skin cancer, J. Am. Acad. Dermatol. 64 (2011) 839–848. doi:10.1016/j.jaad.2010.06.028.

[3] V. Madan, J.T. Lear, R.-M. Szeimies, Non-melanoma skin cancer, Lancet. 375 (2010) 673–685. doi:10.1016/S0140-6736(09)61196-X.

[4] N.R. Telfer, G.B. Colver, C.A. Morton, British Association of Dermatologists, Guidelines for the management of basal cell carcinoma, Br. J. Dermatol. 159 (2008) 35–48. doi:10.1111/j.1365-2133.2008.08666.x.

[5] G. Goldenberg, L.E. Golitz, J. Fitzpatrick, Histopathology of Skin Cancer, in: Manag. Ski. Cancer, Springer Berlin Heidelberg, Berlin, Heidelberg, 2010: pp. 17–35. doi:10.1007/978-3-540-79347-2_2.

[6] A.H. Arits, K. Mosterd, B.A. Essers, E. Spoorenberg, A. Sommer, M.J. De Rooij, H.P. van Pelt, P.J. Quaedvlieg, G.A. Krekels, P.A. van Neer, J.J. Rijzewijk, A.J. van Geest, P.M. Steijlen, P.J. Nelemans, N.W. Kelleners-Smeets, Photodynamic therapy versus topical imiquimod versus topical fluorouracil for treatment of superficial basal-cell carcinoma: a single blind, non-

inferiority, randomised controlled trial, Lancet Oncol. 14 (2013) 647–654. doi:10.1016/S1470-2045(13)70143-8.

[7] J.J. Rippey, Why classify basal cell carcinomas?, Histopathology. 32 (1998) 393–8. http://www.ncbi.nlm.nih.gov/pubmed/9639112 (accessed August 18, 2018).

[8] F. Bath-Hextall, M. Ozolins, S.J. Armstrong, G.B. Colver, W. Perkins, P.S.J. Miller, H.C. Williams, Surgery versus Imiquimod for Nodular Superficial basal cell carcinoma (SINS) study group, Surgical excision versus imiquimod 5% cream for nodular and superficial basal-cell carcinoma (SINS): a multicentre, non-inferiority, randomised controlled trial, Lancet Oncol. 15 (2014) 96–105. doi:10.1016/S1470-2045(13)70530-8.

[9] I. Telo, S. Pescina, C. Padula, P. Santi, S. Nicoli, Mechanisms of imiquimod skin penetration, Int. J. Pharm. 511 (2016) 516–523. doi:10.1016/j.ijpharm.2016.07.043.

[10] P. Stein, K. Gogoll, S. Tenzer, H. Schild, S. Stevanovic, P. Langguth, M.P. Radsak, Efficacy of Imiquimod-Based Transcutaneous Immunization Using a Nano-Dispersed Emulsion Gel Formulation, PLoS One. 9 (2014) e102664. doi:10.1371/journal.pone.0102664.

[11] K. Rehman, M.F.F.M. Aluwi, K. Rullah, L.K. Wai, M.C.I. Mohd Amin, M.H. Zulfakar, Probing the effects of fish oil on the delivery and inflammation-inducing potential of imiquimod, Int. J. Pharm. 490 (2015) 131–141. doi:10.1016/j.ijpharm.2015.05.045.

[12] G.P. Moss, D.R. Gullick, S.C. Wilkinson, Methods for the Measurement of Percutaneous Absorption, in: Predict. Methods Percutaneous Absorpt., Springer Berlin Heidelberg, Berlin, Heidelberg, 2015: pp. 25–42. doi:10.1007/978-3-662-47371-9_2.

578 [13] Y.-C. Kim, J.-H. Park, M.R. Prausnitz, Microneedles for drug and vaccine delivery, Adv. Drug
579 Deliv. Rev. 64 (2012) 1547–1568. doi:10.1016/J.ADDR.2012.04.005.

580 [14] T.M. Tuan-Mahmood, M.T.C. McCrudden, B.M. Torrisi, E. McAlister, M.J. Garland, T.R.R. Singh,
581 R.F. Donnelly, Microneedles for intradermal and transdermal drug delivery, Eur. J. Pharm. Sci.
582 50 (2013) 623–637. doi:10.1016/j.ejps.2013.05.005.

583 [15] K. Van Der Maaden, W. Jiskoot, J. Bouwstra, Microneedle technologies for (trans)dermal drug
584 and vaccine delivery, J. Control. Release. 161 (2012) 645–655.
585 doi:10.1016/j.jconrel.2012.01.042.

586 [16] R.F. Donnelly, D.I.J. Morrow, P.A. McCarron, A.D. Woolfson, A. Morrissey, P. Juzenas, A.
587 Juzeniene, V. Iani, H.O. McCarthy, J. Moan, Microneedle-mediated intradermal delivery of 5-
588 aminolevulinic acid: Potential for enhanced topical photodynamic therapy, J. Control. Release.
589 129 (2008) 154–162. doi:10.1016/j.jconrel.2008.05.002.

590 [17] D. Touboul, A. Brunelle, O. Laprévote, Improvement of Biological Time-of-Flight- Secondary Ion
591 Mass Spectrometry Imaging with a Bismuth Cluster Ion Source, J Am Soc Mass Spectrom. 16
592 (2005) 1608–1618. doi:10.1016/j.jasms.2005.06.005.

593 [18] A.M. Judd, D.J. Scurr, J.R. Heylings, K. Wan, P. Gary, Distribution and Visualisation of
594 Chlorhexidine Within the Skin Using ToF-SIMS : A Potential Platform for the Design of More
595 Efficacious Skin Antiseptic Formulations, Pharm Res. 30 (2013) 1896–1905.
596 doi:10.1007/s11095-013-1032-5.

597 [19] N.J. Starr, D.J. Johnson, J. Wibawa, I. Marlow, M. Bell, D.A. Barrett, D.J. Scurr, Age-Related
598 Changes to Human Stratum Corneum Lipids Detected Using Time-of-Flight Secondary Ion Mass

599 Spectrometry Following in Vivo Sampling, Anal. Chem. 88 (2016) 4400–4408.
600 doi:10.1021/acs.analchem.5b04872.

601 [20] P. Sjövall, T.M. Greve, S.K. Clausen, K. Moller, S. Eirefelt, B. Johansson, K.T. Nielsen, Imaging of
602 distribution of topically applied drug molecules in mouse skin by combination of time-of-flight
603 secondary ion mass spectrometry and scanning electron microscopy, Anal. Chem. 86 (2014)
604 3443–3452. doi:10.1021/ac403924w.

605 [21] T. Kezutyte, N. Desbenoit, A. Brunelle, V. Briedis, Studying the penetration of fatty acids into
606 human skin by ex vivo TOF-SIMS imaging, Biointerphases. 8 (2013) 3. doi:10.1186/1559-4106-
607 8-3.

608 [22] V. Čižinauskas, N. Elie, A. Brunelle, V. Briedis, Fatty acids penetration into human skin *ex vivo* :
609 A TOF-SIMS analysis approach, Biointerphases. 12 (2017) 011003. doi:10.1116/1.4977941.

610 [23] V. Čižinauskas, N. Elie, A. Brunelle, V. Briedis, Skin Penetration Enhancement by Natural Oils for
611 Dihydroquercetin Delivery, Molecules. 22 (2017) 1536. doi:10.3390/molecules22091536.

612 [24] F. Benech-Kieffer, P. Wegrich, R. Schwarzenbach, G. Klecak, T. Weber, J. Leclaire, H. Schaefer,
613 Percutaneous Absorption of Sunscreens in vitro: Interspecies Comparison, Skin Models and
614 Reproducibility Aspects, Skin Pharmacol. Physiol. 13 (2000) 324–335. doi:10.1159/000029940.

615 [25] Y.W. Naguib, A. Kumar, Z. Cui, The effect of microneedles on the skin permeability and
616 antitumor activity of topical 5-fluorouracil., Acta Pharm. Sin. B. 4 (2014) 94–99.
617 doi:10.1016/j.apsb.2013.12.013.

618 [26] D.J. Davies, R.J. Ward, J.R. Heylings, Multi-species assessment of electrical resistance as a skin

619 integrity marker for in vitro percutaneous absorption studies, Toxicol. Vitr. 18 (2004) 351–358.
620 doi:10.1016/j.tiv.2003.10.004.

621 [27] L. Bartosova, J. Bajgar, Transdermal Drug Delivery In Vitro Using Diffusion Cells, Curr. Med.
622 Chem. 19 (2012) 4671–4677. doi:1875-533X/12 $58.00+.00.

623 [28] M.E. Lane, Skin penetration enhancers, Int. J. Pharm. 447 (2013) 12–21.
624 doi:10.1016/j.ijpharm.2013.02.040.

625 [29] J. Lademann, U. Jacobi, C. Surber, H.-J. Weigmann, J.W. Fluhr, The tape stripping procedure –
626 evaluation of some critical parameters, Eur. J. Pharm. Biopharm. 72 (2009) 317–323.
627 doi:10.1016/j.ejpb.2008.08.008.

628 [30] S. Fleury, R.F. Vianna Lopez, Topical Administration of Anticancer Drugs for Skin Cancer
629 Treatment, in: Ski. Cancers - Risk Factors, Prev. Ther., InTech, 2011. doi:10.5772/27785.

630 [31] L. Anne Skelton, The effective treatment of basal cell carcinoma, Br. J. Nurs. 18 (2009) 346–
631 350. doi:10.12968/bjon.2009.18.6.40766.

632 [32] H.I. Maibach, Dermal Absorption Models in Toxicology and Pharmacology, Clin. Toxicol. 45
633 (2007) 736–736. doi:10.1080/15563650701502766.

634 [33] G.P. Moss, D.R. Gullick, S.C. Wilkinson, Predictive methods in percutaneous absorption, Predict.
635 Methods Percutaneous Absorpt. (2015) 1–199. doi:10.1007/978-3-662-47371-9.

636 [34] A. Teichmann, S. Heuschkel, U. Jacobi, G. Presse, R.H.H. Neubert, W. Sterry, J. Lademann,
637 Comparison of stratum corneum penetration and localization of a lipophilic model drug applied

638 in an o/w microemulsion and an amphiphilic cream, Eur. J. Pharm. Biopharm. 67 (2007) 699–
639 706. doi:10.1016/j.ejpb.2007.04.006.

640 [35] E. Chatelain, B. Gabard, C. Surber, Skin Penetration and Sun Protection Factor of Five UV Filters:
641 Effect of the Vehicle, Skin Pharmacol. Physiol. 16 (2003) 28–35. doi:10.1159/000068291.

642 [36] K.L. Trebilcock, J.R. Heylings, M.F. Wilks, In vitro tape stripping as a model for in vivo skin
643 stripping., Toxicol. In Vitro. 8 (1994) 665–7. http://www.ncbi.nlm.nih.gov/pubmed/20692983
644 (accessed August 19, 2018).

645 [37] U. Jacobi, H.-J. Weigmann, J. Ulrich, W. Sterry, J. Lademann, Estimation of the relative stratum
646 corneum amount removed by tape stripping, Ski. Res. Technol. 11 (2005) 91–96.
647 doi:10.1111/j.1600-0846.2005.00094.x.

648 [38] S.J. Bashir, A.L. Chew, A. Anigbogu, F. Dreher, H.I. Maibach, Physical and physiological effects
649 of stratum corneum tape stripping., Skin Res. Technol. 7 (2001) 40–8.
650 http://www.ncbi.nlm.nih.gov/pubmed/11301640 (accessed August 19, 2018).

651 [39] K.M. McKay, B.L. Sambrano, P.S. Fox, R.L. Bassett, S. Chon, V.G. Prieto, Thickness of superficial
652 basal cell carcinoma (sBCC) predicts imiquimod efficacy: a proposal for a thickness-based
653 definition of sBCC, Br. J. Dermatol. 169 (2013) 549–554. doi:10.1111/bjd.12402.

654 [40] F.J. Verbaan, S.M. Bal, D.J. van den Berg, J.A. Dijksman, M. van Hecke, H. Verpoorten, A. van
655 den Berg, R. Luttge, J.A. Bouwstra, Improved piercing of microneedle arrays in dermatomed
656 human skin by an impact insertion method, J. Control. Release. 128 (2008) 80–88.
657 doi:10.1016/j.jconrel.2008.02.009.

658 [41] R.E.M. Lutton, J. Moore, E. Larrañeta, S. Ligett, A.D. Woolfson, R.F. Donnelly, Microneedle
659 characterisation: the need for universal acceptance criteria and GMP specifications when
660 moving towards commercialisation, Drug Deliv. Transl. Res. 5 (2015) 313–331.
661 doi:10.1007/s13346-015-0237-z.

662 [42] S.A. Coulman, J.C. Birchall, A. Alex, M. Pearton, B. Hofer, C. O'Mahony, W. Drexler, B. Považay,
663 In Vivo, In Situ Imaging of Microneedle Insertion into the Skin of Human Volunteers Using
664 Optical Coherence Tomography, Pharm. Res. 28 (2011) 66–81. doi:10.1007/s11095-010-0167-
665 x.

666 [43] H.G. Kaporis, E. Guttman-yassky, M.A. Lowes, A.S. Haider, J. Fuentes-duculan, K. Darabi, J.
667 Whynot-ertelt, A. Khatcherian, I. Cardinale, I. Novitskaya, G. James, J.A. Carucci, Human Basal
668 Cell Carcinoma Is Associated with Foxp3 þ T cells in a Th2 Dominant Microenvironment, J.
669 Invest. Dermatol. 127 (2007) 2391–2398. doi:10.1038/sj.jid.5700884.

670 [44] Y. Ma, S.E. Boese, Z. Luo, N. Nitin, H.S. Gill, Drug coated microneedles for minimally-invasive
671 treatment of oral carcinomas: development and in vitro evaluation, Biomed. Microdevices. 17
672 (2015). doi:10.1007/s10544-015-9944-y.

673 [45] W. Yu, G. Jiang, D. Liu, L. Li, H. Chen, Y. Liu, Q. Huang, Z. Tong, J. Yao, X. Kong, Fabrication of
674 biodegradable composite microneedles based on calcium sulfate and gelatin for transdermal
675 delivery of insulin, Mater. Sci. Eng. C. 71 (2017) 725–734. doi:10.1016/j.msec.2016.10.063.

676